J. Fluid Mech. (1995), vol. 301, pp. 371–382

Three-dimensional convection driven by centrifugal buoyancy

By M. AUER, F. H. BUSSE AND R. M. CLEVER

Institute of Physics, University of Bayreuth, D-95440 Bayreuth
and Institute of Geophysics and Planetary Physics, University of California, Los Angeles, CA 90024, USA

(Received 2 November 1994 and in revised form 11 April 1995)

Convection driven by centrifugal buoyancy in a cylindrical fluid annulus cooled from the inside, heated from the outside, and rotating about its axis is described. While at high values of the dimensionless rotation parameter τ convection rolls aligned with the axis are preferred, three-dimensional patterns of convection are introduced at low values of τ through either the cross-roll instability or a subharmonic varicose instability. The instabilities are studied in terms of simple analytical relationships as well as through numerical methods based on the Galerkin scheme. Analytical expressions for the steady three-dimensional patterns induced by the instabilities are also derived.

1. Introduction

Thermal convection in a fluid layer heated from below in the presence of a parallel axis of rotation is readily realized in the annular gap between two coaxial rotating cylinders kept at different temperatures such that the density stratification is unstable with respect to the action of the centrifugal force. Since the density of fluids typically decreases with increasing temperature the temperature T_1 of the inner cylinder must be kept lower than the temperature T_2 of the outer cylinder in order that the instability can occur. Ordinary gravity exerts a minimal influence on the laboratory experiment when the orientation of the cylindrical annulus is vertical (Busse & Carrigan 1974).

Convection flows that are driven by buoyancy forces and which are oriented at a right angle with respect to the axis of rotation typically occur in the equatorial regions of the atmospheres of the major planets and of stars. Since the component of gravity parallel to the axis of rotation usually exerts only a minor influence, the equatorial type of convection is representative of the entire region outside the cylindrical surface touching at its equator an inner spherical boundary corresponding, for instance, to a planetary core. Models for convection in the atmospheres of the major planets that are based on the assumption of nearly two-dimensional columnar convection modes have been quite successful in explaining the band structures of Jupiter and Saturn (Busse 1976, 1983, 1988, 1994) and have motivated experimental and theoretical studies of columnar convection in the cylindrical annulus (Busse & Hood 1983; Azouni, Bolton & Busse 1984; Busse & Or 1986; Or & Busse 1987; Schnaubelt & Busse 1992). In all of these studies the limit of high rotation rates has been emphasized in which the nearly two-dimensional character is enforced by the approximate balance between Coriolis force and pressure gradient. The opposite limit

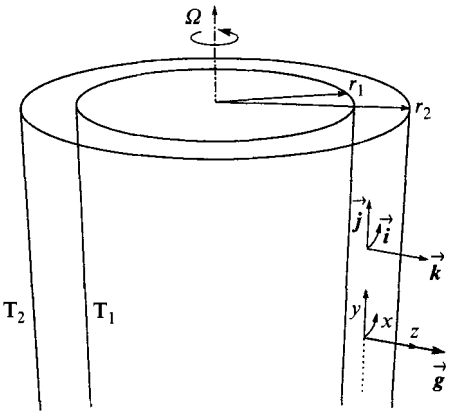

FIGURE 1. Geometrical configuration of the problem.

of low Taylor numbers is of lesser interest for planetary applications, but deserves some attention for the explanation of laboratory observations. Three-dimensional convection flows have been observed (Busse & Carrigan 1974), but little attention has been devoted to them. In the present paper we plan to investigate the problem from a theoretical point of view using both a weakly nonlinear analysis based on amplitude equations and numerical computations based on the Galerkin method. Through these two complementary approaches the realization of two types of three-dimensional patterns will be demonstrated.

The paper starts with a brief formulation of the basic equations in §2. In §3 the weakly nonlinear analysis will be formulated and two types of three-dimensional solutions will be considered in §§4 and 5. Comparisons of the weakly nonlinear results with a numerical analysis of the fully nonlinear problem will be given in §6 for special values of the Prandtl number. The paper closes with an outlook on possible experimental realisations in the concluding section.

2. Mathematical formulation of the problem

We consider the fluid-filled gap between two coaxial co-rotating cylinders of length L with radii r_1 and r_2, respectively, as shown in figure 1. We assume the limit of a large aspect ratio L/d where $d = r_2 - r_1$ is the gap width. We also assume the small gap limit, $d \ll r_1$, which allows us to introduce a Cartesian coordinate system with the origin located in the middle of the gap and the z-coordinate directed in the radial direction of the unit vector $\boldsymbol{k}$. Since we use the centrifugal acceleration as our effective gravity, the latter is directed parallel to $\boldsymbol{k}$. The y-direction is chosen in the direction of the unit vector $\boldsymbol{j}$ parallel to the axis of rotation. The cylinders are held at constant temperatures T_1 and T_2 with $T_1 < T_2$.

Using the general representation for the solenoidal velocity field $\boldsymbol{u}$

$$\boldsymbol{u} = \bar{\boldsymbol{u}} + \nabla \times (\boldsymbol{k} \times \nabla\phi) + \nabla \times \boldsymbol{k}\psi, \tag{1}$$

where the bar indicates the average over the horizontal (x, y)-plane, we obtain the following equations for ϕ and ψ by taking the z-components of the curlcurl and of the curl of the equations of motion:

$$\left[P^{-1}\frac{\partial}{\partial t}-\nabla^2\right]\nabla^2\Delta_2\phi-2\tau\boldsymbol{j}\cdot\nabla\Delta_2\psi+\Delta_2\theta=-\boldsymbol{k}\cdot\nabla\times\nabla\times(\boldsymbol{u}\cdot\nabla\boldsymbol{u})P^{-1}, \tag{2a}$$

$$2\tau\boldsymbol{j}\cdot\nabla\Delta_2\phi+\left[P^{-1}\frac{\partial}{\partial t}-\nabla^2\right]\Delta_2\psi=\boldsymbol{k}\cdot\nabla\times(\boldsymbol{u}\cdot\nabla\boldsymbol{u})P^{-1}, \tag{2b}$$

$$\left[\nabla^2-\frac{\partial}{\partial t}\right]\theta-R\Delta_2\phi=\boldsymbol{u}\cdot\nabla\theta, \tag{2c}$$

with the horizontal Laplacian $\Delta_2=\nabla^2-\partial^2/\partial z^2$. Equation (2c) represents the heat equation for the deviation θ of the temperature field from the static solution.

The mean flow $\bar{\boldsymbol{u}}$ is governed by the equation

$$\left[\frac{\partial^2}{\partial z^2}-P^{-1}\frac{\partial}{\partial t}\right]\bar{\boldsymbol{u}}=-\frac{\partial}{\partial z}\overline{\left[\Delta_2\phi(\nabla_2\frac{\partial\phi}{\partial z}+\nabla\times\boldsymbol{k}\psi)\right]}P^{-1}, \tag{2d}$$

where $\nabla_2=\nabla-\boldsymbol{k}\partial/\partial z$ is the horizontal nabla operator. The term horizontal is used here with respect to the effective gravity even though an experimental realization of the physical system in a laboratory may employ 'vertical' cylinders. The boundary conditions are given by

$$\bar{\boldsymbol{u}}=\phi=\frac{\partial\phi}{\partial z}=\psi=\theta=0 \text{ at } z=\pm0.5. \tag{3}$$

The length, time and temperature in equations (2) are measured in terms of $[d]$, $[d^2/\nu]$, and $[(T_2-T_1)/R]$, respectively. The dimensionless parameters are the Rayleigh number R, the Prandtl number P and the rotation parameter τ defined by

$$R\equiv\gamma(T_2-T_1)\Omega^2(r_1+r_2)d^3/2\nu\kappa,\quad P\equiv\nu/\kappa,\quad \tau\equiv\Omega d^2/\nu,$$

where γ,ν and κ are the thermal expansivity, the kinematic viscosity and the thermal diffusivity, respectively. The system derived here is identical to the Rayleigh–Bénard system with solid boundaries, when the rotation parameter vanishes. This property offers the opportunity of discussing the present system in comparison with the latter one.

The linear problem which governs the stability boundaries of the basic state $\boldsymbol{u}\equiv\theta\equiv0$, is found by neglecting the right-hand sides of (2). The resulting linear system does not depend explicitly on x,y and t. We are thus led to the ansatz of the form $\boldsymbol{X}=\boldsymbol{X}_0(z)\exp(\mathrm{i}(\alpha x+\beta y)+\sigma t)$ with $\boldsymbol{X}=(\phi,\psi,\theta)$. These solutions describe convection rolls with wavevectors $\boldsymbol{q}=(\alpha,\beta)$ and growth rates σ.

Actually the linear stability analysis can be reduced to the stability problem of the Rayleigh–Bénard system, when we restrict it to the onset of monotonic modes, i.e. $\sigma\equiv0$. This restriction is certainly justified in the case of small τ which is of interest to us. Oscillatory modes of onset of convection can be expected for large values of τ when inertial wave-like modes may become possible. For $\sigma=0$ equations. (2) with vanishing right-hand sides can be reduced to the equation

$$\left[\nabla^6-R\Delta_2+4\tau^2\frac{\partial^2}{\partial y^2}\right]\Delta_2\phi=0 \tag{4}$$

with the boundary conditions

$$\phi = \frac{\partial \phi}{\partial z} = \left(\frac{\partial^2}{\partial z^2} - |\boldsymbol{q}|^2\right)^2 \phi = 0 \text{ at } z = \pm 0.5. \tag{5}$$

Thus the critical Rayleigh numbers can be calculated from the critical Rayleigh numbers $R_{RB}(|\boldsymbol{q}|)$ of the Rayleigh–Bénard system (cf. e.g. Busse 1971) according to the relationship

$$R_0(\boldsymbol{q}) = R_{RB}(|\boldsymbol{q}|) + \frac{4\beta^2\tau^2}{|\boldsymbol{q}|^2}. \tag{6}$$

The most unstable modes are axially oriented convection columns with $\boldsymbol{q}_0 = (\alpha_c, 0) = (3.11632, 0)$. The onset occurs at $R_c = 1707.762$. The linear and nonlinear two-dimensional properties of these modes are identical to those of the corresponding modes in Rayleigh-Bénard convection. We thus know that they bifurcate supercritically and a weakly nonlinear approach is possible to determine the convection amplitude at slightly supercritical values of R.

3. Amplitude equations in the weakly nonlinear limit

In the following sections we shall consider several patterns of convection in the weakly nonlinear limit of equations (2). For this purpose the solution vector $\boldsymbol{X}$ is expanded in powers of the amplitudes A_i of the contributing modes of convection:

$$\boldsymbol{X} = \sum_{i=-N}^{N} A_i \boldsymbol{X}_i \exp\{\mathrm{i}\boldsymbol{q}_i \cdot \boldsymbol{r}\} + \sum_{i,k} A_i A_k \boldsymbol{X}_{ik} \exp\{\mathrm{i}(\boldsymbol{q}_i + \boldsymbol{q}_k)\cdot \boldsymbol{r}\} + \text{h.o.t.} \tag{7a}$$

where the summation is extended over positive as well as negative subscripts i,k with the convention

$$A_{-i} = A_i^*, \quad \boldsymbol{q}_{-i} = -\boldsymbol{q}_i, \quad \boldsymbol{q}_i = (\alpha_i, \beta_i). \tag{7b}$$

In order to allow for competing modes corresponding to different wave vectors $\boldsymbol{q}$ we shall assume the limit of small τ^2 such that terms of the order τ^2 will be considered on the same level as terms of the order $|A_i|^2$. After inserting expansion (7) into equations (2), solving the inhomogeneous ordinary differential equations in z for the vector functions $\boldsymbol{X}_{ik}$, we obtain as solvability conditions in the cubic order a system of amplitude equations of the form

$$M_i \frac{\mathrm{d}}{\mathrm{d}t} A_i = (R - R_0(\boldsymbol{q}_i) - \sum_k \gamma_{ik} |A_k|^2) A_i - \sum_{kl} \eta_{ikl} \delta(\boldsymbol{q}_{-i} + \boldsymbol{q}_k + \boldsymbol{q}_l) A_k A_l \tag{8}$$

$$\text{for } i = -N, \ldots, -1, 1, \ldots, N$$

where a weak time dependence of the amplitudes has been assumed and where the constants M_i are defined by

$$M_i = \left\langle |\theta_i|^2 - P^{-1} |\boldsymbol{q}_i|^2 \phi_i \left(\frac{\mathrm{d}^2}{\mathrm{d}z^2} - |\boldsymbol{q}_i|^2\right) \phi_i \right\rangle \langle \theta_i | \boldsymbol{q}_i |^2 \phi_i \rangle^{-1} \tag{9}$$

and the more complex constants γ_{ik}, η_{ikl} are not given explicitly. The angular brackets in (9) indicate the spatial average over the fluid layer. Since deviations from the

Boussinesq approximation are not included in the present analysis and since symmetric boundary conditions are employed, the constants η_{ikl} vanish in the limit $\tau = 0$. For finite τ, however, values of η_{ikl} in proportion to τ arise whenever the vector sum $\boldsymbol{q}_k + \boldsymbol{q}_l - \boldsymbol{q}_i$ vanishes as indicated by the δ-function.

In the special case of steady roll convection with $\boldsymbol{q}_1 = (\alpha_c, 0)$ the amplitude A_1 of convection is given by

$$A_1^2 = (R - R_c)/2\gamma_{11} \tag{10}$$

where $\gamma_{11} = \gamma_0 + \tau^2\gamma_1 + \ldots$ is given in the limit $\tau = 0$ by

$$\gamma_0 \equiv (0.69942 - 0.00472P^{-1} + 0.00832P^{-2})^{-1} \tag{11}$$

according to Schlüter, Lortz & Busse (1965) when the normalization condition

$$R_0(\boldsymbol{q}_i)\langle\theta_i \mid \boldsymbol{q}_i \mid^2 \phi_i\rangle = 1 \tag{12}$$

is employed.

4. Knot convection

The simplest case of three-dimensional convection described by the system (8) of amplitude equations arises for two participating modes, the $\boldsymbol{q}$-vectors of which are oriented at right angles:

$$\boldsymbol{q}_1 = (\alpha_c, 0), \quad \boldsymbol{q}_2 = (0, \alpha_c) \tag{13}$$

The amplitude equations (8) can be simplified in this case:

$$M_1 \frac{\mathrm{d}}{\mathrm{d}t} A_1 = (R - R_c - 2\gamma_{11}A_1^2 - 2\gamma_{12}A_2^2)A_1, \tag{14a}$$

$$M_1 \frac{\mathrm{d}}{\mathrm{d}t} A_2 = (R - R_c - 4\tau^2 - 2\gamma_{22}A_2^2 - 2\gamma_{21}A_1^2)A_2. \tag{14b}$$

The solution in the form of rolls (10) with $A_2 = 0$ is a stable solution of (14) in the range $R_c \leqslant R < R_{CR}$. At the critical Rayleigh number R_{CR} for the onset of cross-roll disturbances

$$R_{CR} = R_c + \frac{4\tau^2}{1 - \gamma_{21}/\gamma_{11}} \quad \text{for} \quad \frac{\gamma_{21}}{\gamma_{11}} < 1 \tag{15}$$

a solution with finite amplitude A_2 bifurcates and replaces the roll solution as the stable solution of the system (14). For $\tau = 0$, however, the condition $\gamma_{21} < \gamma_{11}$ is not satisfied since

$$\gamma_{21} - \gamma_{11} = 0.15901 + 0.08973P^{-1} + 0.11661P^{-2} \equiv a_0\gamma_{11} \tag{16}$$

according to Busse (1971). When terms of the order τ^2 are taken into account we find

$$\frac{\gamma_{21} - \gamma_{11}}{\gamma_{11}} = a_0 - a_2\tau^2 + \ldots \tag{17}$$

with a_2 given in figure 2 as a function of the Prandtl number. Accordingly the cross-roll instability occurs when $\mid \tau \mid$ exceeds a critical value τ_c:

$$\mid \tau \mid \geqslant \tau_c \equiv (a_0/a_2)^{1/2} \tag{18}$$

which varies between 7 for low Prandtl numbers and 3.6 in the limit $P \to \infty$.

Obviously the results (15), (17), (18) are not rigorous in any mathematical sense.

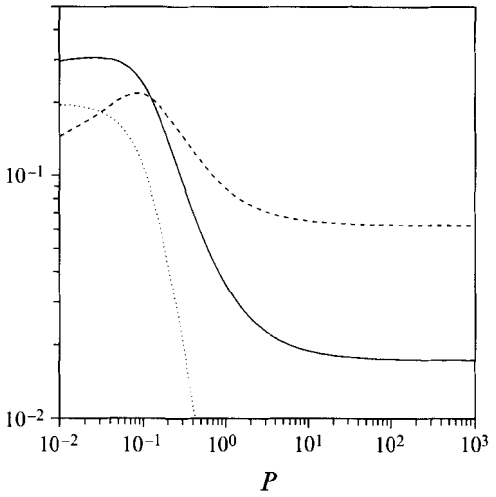

FIGURE 2. The coefficients a_2 (solid line), b_2 (dashed line) and c_2 (dotted line) as functions of the Prandtl number P. The coefficients are defined in equations (17), (19).

But since the change in the critical value (6) of the Rayleigh number is still a small fraction of R_c for $\tau = \tau_c$ and since the stability boundary (15) agrees quite well with the numerical solutions of the fully nonlinear equations to be discussed in §6, we feel that the analytical result provides a good approximation. The fair agreement encourages us to go a step further and to calculate the amplitudes A_1, A_2 of the steady three-dimensional solution describing knot convection. For this purpose the remaining coefficients γ_{12} and γ_{22} must be determined. Using the definition

$$\left.\begin{aligned} \gamma_{12}/\gamma_{11} - 1 &= a_0 + b_2\tau^2 + \ldots, \\ \gamma_{22}/\gamma_{11} - 1 &= -c_2\tau^2 + \ldots \end{aligned}\right\} \tag{19}$$

we have plotted b_2 and c_2 as function of P in figure 2. Since c_2 is rather small we can neglect it to a first approximation and arrive at the solution for knot convection:

$$|A_1|^2 = [(a_0 + b_2\tau^2)(R - R_c - 4\tau^2) - 4\tau^2]/D, \tag{20a}$$

$$|A_2|^2 = [(a_0 - a_2\tau^2)(R - R_c) + 4\tau^2]/D, \tag{20b}$$

with $D = 2\gamma_{11}[(1 + a_0 + b_2\tau^2)(1 + a_0 - a_2\tau^2) - 1]$.

5. Subharmonic varicose instability and transition to hexaroll convection

In this section we consider the simplest case of the system (8) of amplitude equations in which the terms bilinear in A_i contribute. For this purpose three $\boldsymbol{q}$-vectors of the form $\boldsymbol{q}_1 = (\alpha_c, 0), \boldsymbol{q}_2 = (\alpha_c/2, \beta), \boldsymbol{q}_3 = (\alpha_c/2, -\beta)$ will be chosen where β is given by $\sqrt{3}\alpha_c/2$, at least in the case $\tau = 0$. In the latter case hexagonal convection in its two manifestations of up- and down-hexagons corresponds to steady – but unstable – solutions of equations (8). Here we investigate the possibility that similar solutions may become stable for finite values of τ. For this purpose equations (8) can be rewritten in the form

$$M_1 \frac{\mathrm{d}}{\mathrm{d}t} A_1 = (R - R_c - \sum_{k=1}^{3} \gamma_{1k} \mid A_k \mid^2) A_1 + \mathrm{i}\eta_1 \tau A_2 A_3, \tag{21a}$$

$$M_2 \frac{\mathrm{d}}{\mathrm{d}t} A_2 = (R - R_c - 3\tau^2 - \sum_{k=1}^{3} \gamma_{2k} \mid A_k \mid^2) A_2 + \mathrm{i}\eta_2 \tau A_1 A_3^*, \tag{21b}$$

$$M_2 \frac{\mathrm{d}}{\mathrm{d}t} A_3 = (R - R_c - 3\tau^2 - \sum_{k=1}^{3} \gamma_{3k} \mid A_k \mid^2) A_3 + \mathrm{i}\eta_2 \tau A_1 A_2^*, \tag{21c}$$

The stability analysis of the steady roll solution (10) with respect to infinitesimal disturbances $A_j = \tilde{A}_j \exp\{\sigma t\}$, $j = 2, 3$ yields for the growth rate

$$M_2 \sigma = \pm \tau \eta_2 [(R - R_c)/\gamma_{11}]^{1/2} + (R - R_c)(1 - \gamma_{21}/\gamma_{11}) - 3\tau^2. \tag{22}$$

Accordingly the two-dimensional roll solution is unstable in the range

$$R_- < R < R_+ \tag{23a}$$

with

$$R_\pm - R_c \equiv \left\{ \eta_2 / 2h_0 \gamma_{11}^{1/2} \pm \left(\eta_2^2 / 4h_0^2 \gamma_{11} - 3/h_0 \right)^{1/2} \right\}^2 \tau^2 \tag{23b}$$

provided the expression under the square root is positive, i.e.

$$\eta_2^2 > 12 h_0 \gamma_{11} \tag{24}$$

where h_0 is defined by

$$\gamma_{ij} - \gamma_{11} = h_0 \gamma_{11} (1 - \delta_{ij}) + \ldots \equiv (0.29127 + 0.08147 P^{-1} + 0.08933 P^{-2})(1 - \delta_{ij}) + \ldots \tag{25}$$

Here we have neglected contributions of the order τ^2 to γ_{11} since they are of higher order than those retained in expressions (23). The evaluation of inequality (24) demonstrates that it is satisfied for $P > 2.95$. In figure 3 we have plotted $R_\pm - R_c$ as function of the Prandtl number. Also shown in that figure are the coefficients η_1 and η_2.

In order to distinguish the new instability from the hexagon instability caused by deviations from the Boussinesq approximation (Busse 1967) we have called it the subharmonic varicose instability. Indeed, the evolution of this instability does not cause a transition to a hexagon solution, but instead it just causes a varicose deformation of the roll pattern which shifts by half a wavelength along the axis of the rolls from one pair of rolls to the next. Based on the solution of equations (21) such a hexaroll solution has been plotted in figure 4.

In order to derive an expression for the hexaroll solution we assume that A_1 is real and given by the expression (10) to a first approximation. Equations (21*b*,c) can then be solved for small real values of $A_2 = \mathrm{i}A_3$,

$$A_2^2 = \sigma_H M_2 (\gamma_{11} + \gamma_{21})^{-1} \tag{26}$$

where σ_H denotes expression (22) for σ in the case of the positive sign. The maximum value of σ_H and thus the maximum amplitude A_2 is obtained for

$$R_m = R_c + \eta_2 / 2h_0 \gamma_{11}^{1/2} \tag{27}$$

But even at this Rayleigh number the ratio $\mid A_2/A_1 \mid$ stays less than 0.5. For figure

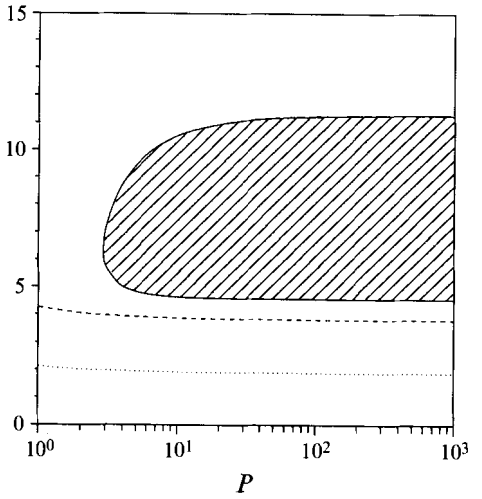

FIGURE 3. $(R_\pm - R_c)\tau^{-2}$ as function of P. The shaded area indicates the region where a finite interval $R_- < R < R_+$ exits. The coefficients η_1 (dashed line) and η_2 (dotted line) are also shown.

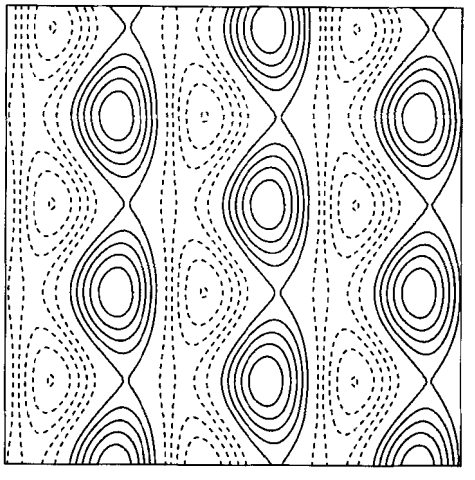

FIGURE 4. Lines of constant azimuthal velocity $\boldsymbol{i}\cdot\boldsymbol{u}$ in the plane $z = 0.4$ for the hexaroll solution at $R = R_m$. Lines with positive (negative) velocity are solid (dashed) for positive τ.

4 $R = R_m$ has been used. At other values R within that interval the primary roll component will dominate even more strongly.

6. Numerical analysis

The numerical analysis of the stability of rolls based on equations (2) follows previous work on the transitions from two- to three-dimensional convection flows in a layer heated from below with horizontal anisotropies. Examples are the instabilities of longitudinal rolls in the presence of a mean shear (Clever, Busse & Kelly 1977; Clever & Busse 1989, 1991) or in the presence of a horizontal magnetic field (Busse & Clever 1983, 1989). The latter example is particularly close to the present situation since no advection effects due to mean flows are involved.

Using the representation for the velocity field $\boldsymbol{u}$ we describe two-dimensional rolls

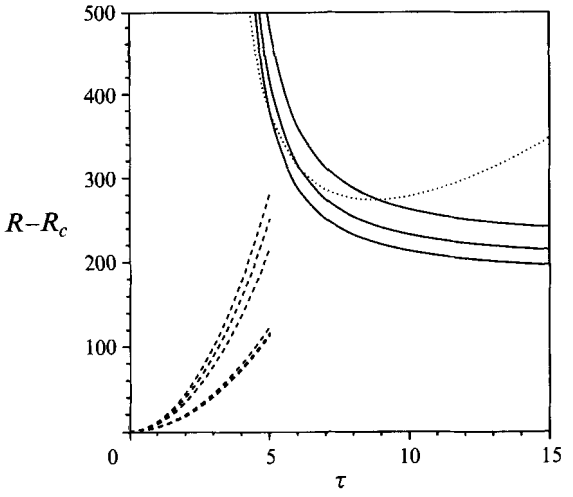

FIGURE 5. Approximate stability boundaries as a function R and τ for the Prandtl numbers 4,7 and 1000 according to criteria (15) (solid lines) and (23) (dashed lines). Rolls with the critical wavenumber α_c are unstable beyond the solid lines with respect to growing cross-roll disturbances and inside the region bounded by the two sets of dashed lines they are unstable with respect to the subharmonic varicose instability. In the latter case the unstable region spreads in both directions with increasing Prandtl number, and the region of unstable rolls also increases with P in the case of the knot instability. The dotted line represents the numerically determined stability boundary for $P = 7$.

in the form

$$\phi = \sum_{l,n} a_{ln} \cos l\alpha_x x \;\; g_n(z), \quad \psi \equiv 0, \tag{28a}$$

$$\theta = \sum_{l,n} b_{ln} \cos l\alpha_x x \;\; \sin n\pi(z + \tfrac{1}{2}), \tag{28b}$$

where $g_n(z)$ are the Chandrasekhar functions (Chandrasekhar 1961) which satisfy the boundary conditions $\phi = \partial\phi/\partial z = 0$ at $z = \pm\frac{1}{2}$. The stability equations for general infinitesimal disturbances can then be solved with the ansatz

$$\tilde{\phi} = \sum_{l,n} \tilde{a}_{ln} \exp\{\mathrm{i}(l\alpha_x + d)x + \mathrm{i}by + \sigma t\} g_n(z), \tag{29a}$$

$$\tilde{\psi} = \sum_{l,n} \tilde{c}_{ln} \exp\{\mathrm{i}(l\alpha_x + d)x + \mathrm{i}by + \sigma t\} \sin n\pi(z + \tfrac{1}{2}), \tag{29b}$$

$$\tilde{\theta} = \sum_{l,n} \tilde{b}_{ln} \exp\{\mathrm{i}(l\alpha_x + d)x + \mathrm{i}by + \sigma t\} \sin n\pi(z + \tfrac{1}{2}) \tag{29c}$$

where the growth rate σ can be determined as the eigenvalue in the system of linear homogeneous equations for the coefficients $\tilde{a}_{ln}, \tilde{c}_{ln}, \tilde{b}_{ln}$. Whenever there exists as a function of the wavenumbers b, d an eigenvalue σ with positive real part, the steady solution (26) characterized by the parameters R, P, α_x will be considered unstable. Otherwise it is regarded as stable.

The stability boundaries obtained through this procedure are shown in figure 5. As expected according to the analytical theory outlined above, the most strongly growing disturbances at low Rayleigh numbers close to R_c correspond to either $d = 0, b \approx \alpha_c$

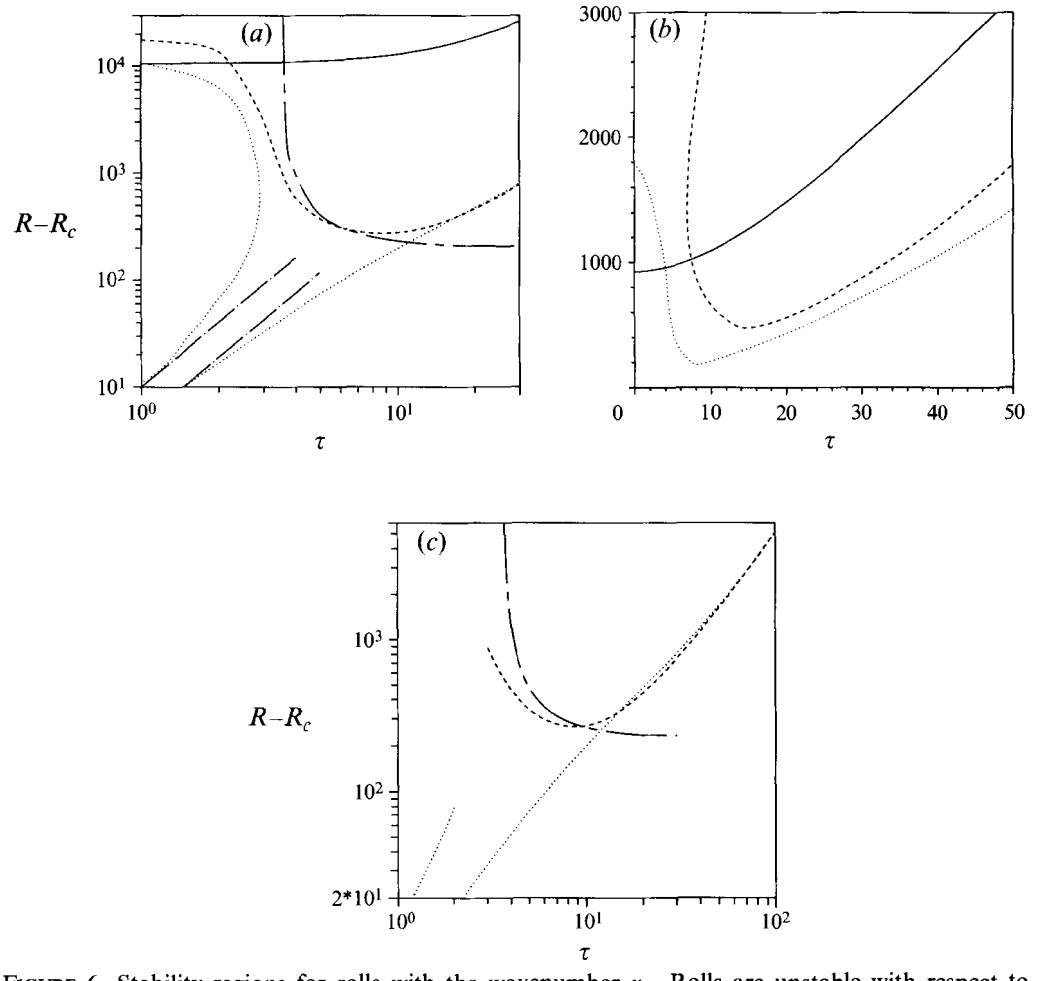

FIGURE 6. Stability regions for rolls with the wavenumber α_c. Rolls are unstable with respect to the subharmonic varicose instability in the region between the two (or above the) dotted lines (the analytical criterion (23) corresponds to the dash-dotted lines). They are also unstable with respect to the knot instability (cross-roll disturbances) indicated by the dashed line. The approximate criterion (15) is indicated by the long-dash-short-dash line. Finally the onset of skewed varicose disturbances is indicated by the solid line. (*a*) $P = 7$, (*b*) $P = 0.71$, (*c*) $P = 1000$.

(cross-roll disturbances) or to the subharmonic skewed varicose disturbances with $d = \alpha/2, b \approx \sqrt{3}\alpha_c/2$. The rather sudden onset of growing cross-roll disturbances with increasing rotation parameter is clearly exhibited in figure 5. In figure 6(*a*) the stability boundary is continued at higher Rayleigh number to the limit $\tau \to 0$ where the instability is known to lead to knot convection (Clever & Busse 1989). Since a similar convection pattern is expected in the case of finite τ the name knot convection has been retained.

While the criterion (15) provides only a rough approximation for the knot stability boundary, the agreement between the analytical expression (23) and the numerical results becomes exact when the critical value R_c of the Rayleigh number is approached as shown in figure 6(*a*). For Prandtl numbers less than 2.95 rolls become stable in the neighbourhood of $R = R_c$, but the subharmonic varicose instability continues to restrict the stability of rolls at somewhat higher Rayleigh numbers as is evident from

stability boundaries for $P = 0.71$ which are shown in figure 6(*b*). For completeness the stability boundary for the onset of the skewed varicose instability (Busse & Clever 1979) is also shown in figure 6(*a*,b). It is preceded by the onset of the instabilities discussed above except for very small values of τ.

From figure 6(*a*,b) it is not quite clear whether the knot instability ever occurs below the onset of the subharmonic varicose instability for $\tau \geqslant 10$. Both stability boundaries are surprisingly close in this regime for Prandtl numbers of the order one and larger. The detailed computations for the case $P = 1000$ shown in figure 6(*c*) demonstrate, however, that the onset of cross-roll disturbances precedes the onset of the subharmonic varicose instability for a finite range of τ.

7. Concluding remarks

For the experimental investigation of the instabilities considered in this paper and the three-dimensional convection flows they generate, a highly viscous fluid contained in the narrow annular gap between two coaxial cylinders should be used. The high viscosity will keep the parameter τ sufficiently small even in the limit when the cylindrical apparatus rotates about its vertical axis rather rapidly, such that the centrifugal force greatly exceeds gravity. Visualizations of the convection patterns can be done with the use of Kalliroscope^R platelets immersed in the fluid. The orientation of the platelets is very sensitive to the shear and has been used in earlier experiments to determine the onset of convection (Busse & Carrigan, 1974). No report of experimental observations of this kind in the relevant parameter regime are known to the authors and it is planned for this reason to undertake a laboratory experiment in the future.

Both instabilities investigated in the paper are caused by the introduction of a z-component of the vorticity. This component of vorticity is at most of order A^3 in the isotropic Rayleigh–Bénard layer when deviations of the order A of the wavenumber from the critical value α_c are admitted, where A denotes the amplitude of convection (see, for example, Schlüter *et al.* 1965). In the present case this component is of the order $A\tau$ and is thus capable of introducing a new instability even at the critical Rayleigh number in the case of subharmonic varicose disturbances.

The research reported in this paper has been supported in part by the Deutsche Forschungsgemeinschaft (M.A.) and by the US National Science Foundation (R.M.C.) and by a NATO travel grant (F.H.B.).

REFERENCES

AZOUNI, A., BOLTON, E. W. & BUSSE, F. H. 1986 Experimental study of convection columns in a rotating cylindrical annulus. *Geophys. Astrophys. Fluid Dyn.* **34**, 301–317.

BUSSE, F. H. 1967 The stability of finite amplitude cellular convection and its relation to an extremum principle. *J. Fluid Mech.* **30**, 625–649.

BUSSE, F. H. 1971 Stability regions of cellular fluid flow. In *Proc. IUTAM Symp. on Instability of Continuous Systems, Herrenalb, 1969* (ed. H. Leipholz), pp. 41–47. Springer.

BUSSE, F. H. 1976 A simple model of convection in the Jovian atmosphere. *Icarus* **20**, 255–260.

BUSSE, F. H. 1983 Convection driven zonal flows in the major planets. *Pageoph* **121**, 375–390.

BUSSE, F. H. 1988 Atmospheric dynamics of the major planets. In *The Physics of the Planets* (ed. S. K. Runcorn), pp. 173–183. John Wiley & Sons.

BUSSE, F. H. 1994 Convection driven zonal flows and vortices in the major planets. *Chaos* **4**, 123–134.

BUSSE, F. H. & CARRIGAN, C. R. 1974 Convection induced by centrifugal buoyancy. *J. Fluid Mech.* **62**, 579–592.

BUSSE, F. H. & CLEVER, R. M. 1979 Instabilities of convection rolls in a fluid of moderate Prandtl number. *J. Fluid Mech.* **91**, 319–335.

BUSSE, F. H. & CLEVER, R. M. 1983 Stability of convection rolls in the presence of a horizontal magnetic field. *J. Méc. Théor. Appl.* **2**, 495–502.

BUSSE, F. H. & CLEVER, R. M. 1989 Traveling wave convection in the presence of a horizontal magnetic field. *Phys. Rev.* A **40**, 1954–1961.

BUSSE, F. H. & HOOD, L. L. 1982 Differential rotation driven by convection in a rotating annulus. *Geophys. Astrophys. Fluid Dyn.* **21**, 59–74.

BUSSE, F. H. & OR, A. C. 1986 Convection in a rotating cylindrical annulus Part 1. Thermal Rossby waves. *J. Fluid Mech.* **166**, 173–187.

CHANDRASEKHAR, S. 1961 *Hydrodynamic and Hydromagnetic Stability.* Clarendon Press.

CLEVER, R. M. & BUSSE, F. H. 1989 Three-dimensional knot convection in a layer heated from below. *J. Fluid Mech.* **198**, 345–363.

CLEVER, R. M. & BUSSE, F. H. 1991 Instabilities of longitudinal rolls in the presence of Poiseuille flow. *J. Fluid Mech.* **229**, 517–529.

CLEVER, R. M., BUSSE, F. H. & KELLY, R. E. 1977 Instabilities of longitudinal convection rolls in Couette flow. *Z. Angew. Math. Phys.* **28**, 771–783.

OR, A. C. & BUSSE, F. H. 1987 Convection in a rotating cylindrical annulus. Part 2. Transitions to asymmetric and vacillating flow. *J. Fluid Mech.* **174**, 313–326.

SCHLÜTER, A., LORTZ, D. & BUSSE, F. 1965 On the stability of steady finite amplitude convection. *J. Fluid Mech.* **23**, 129–144.

SCHNAUBELT, M. & BUSSE, F. H. 1992 Convection in a rotating cylindrical annulus. Part 3. Vacillating and spatially modulated flow. *J. Fluid Mech.* **245**, 155–173.